In situ determination of the water condensation mechanisms on superhydrophobic and superhydrophilic titanium dioxide nanotubes

Manuel Macias-Montero,[1] Carmen Lopez-Santos,[1] A. Nicolas Filippin,[1] Victor J. Rico,[1] Juan P. Espinos,[1] Jordi Fraxedas,[2] Virginia Perez-Dieste,[3] Carlos Escudero,[3] Agustin R. Gonzalez-Elipe[1] and Ana Borras[1]**

(1) Nanotechnology on Surfaces Laboratory, Materials Science Institute of Seville (CSIC-US), Américo Vespucio 49. 41092 - Seville (Spain), (2) Catalan Institute of Nanoscience and Nanotechnology (CSIC-ICTB), Campus de la UAB, 08193-Bellaterra (Spain) and (3) Alba Synchrotron Light Source Carretera BP 1413, Km. 3.3, 08290-Cerdanyola del Vallès, Barcelona (Spain).

KEYWORDS. TiO_2 nanotubes, wetting, water condensation, superhydrophilicity, superhydrophobicity, ESEM, NAPP.

ABSTRACT. One-dimensional (1D) nanostructured surfaces based on high-density arrays of nanowires and nanotubes of photoactive titanium dioxide (TiO_2) present a tunable wetting behavior from superhydrophobic to superhydrophilic states. These situations are depicted in a reversible way by simply irradiating with ultraviolet light (superhydrophobic to superhydrophilic) and storage in dark. In this article, we combine in-situ Environmental Scanning Electron

Microscopy (ESEM) and Near Ambient Pressure Photoemission analysis (NAPP) to understand this transition. These experiments reveal complementary information at microscopic and atomic level reflecting the surface wettability and chemical state modifications experienced by these 1D surfaces upon irradiation. We pay a special attention to the role of the water condensation mechanisms and try to elucidate the relationship between apparent water contact angles of sessile drops under ambient conditions at the macroscale with the formation of droplets by water condensation at low temperature and increasing humidity on the nanotubes surfaces. Thus, for the as-grown nanotubes, we reveal a metastable and superhydrophobic Cassie state for sessile drops that tunes towards water dropwise condensation at the microscale compatible with a partial hydrophobic Wenzel state. For the UV irradiated surfaces, a filmwise wetting behavior is observed for both condensed water and sessile droplets. NAPP analyses show a hydroxyl accumulation on the as-grown nanotubes surfaces during the exposure to water condensation conditions, whereas the water filmwise condensation on a previously hydroxyl enriched surface is proved for the superhydrophilic counterpart.

Introduction

Smart surfaces, equipment for power generation or lab-on-a-chip devices are examples of industrial applications where vapor condensation plays a critical role.[1-4] Implications are presented, for example, in the fabrication of water harvesting materials and heat and mass transfer performance of surfaces[3,5] controlled by either filmwise or dropwise condensation. In these and other systems, particularly when involving elements at the nanoscale, the wetting behavior of micro- and nano-structured surfaces and the condensation regimes onto them is yet not fully understood.[3,6,7] Particularly, there is a significant gap in the description of the water

condensation at the nano and microscales and the eventual wetting behavior (and apparent contact angle) at meso and macroscales.[7-8] Nanostructured surfaces with a dual-scaled roughness described by a Cassie-Baxter state[9] are known to depict a dropwise condensation, where droplets with typical radius below 10 μm can be easily removed through a self-propelling mechanism.[10-12] Meanwhile, a detriment in water repellency is found when a high density of surface sites induces water coalescence and permeation in a partial Wenzel state.[11] In more general terms, wetting states of nanostructured systems have been also described as a modified Cassie-Baxter state, although the rich phenomenology encountered in these systems is far from being well understood.[13-16] Specially critical because of their applications in transport and architecture is the fabrication of antifogging, self-cleaning and anti-freezing surfaces[16-20] and the elucidation of the relationship between hydrophobicity/hydrophilicity and freezing-delaying and anti-freezing behaviors.[20-22] Advances in the liquid manipulation at small scales such as in microfluidic devices and for microdroplets transferring are also conditioned to the condensation and wetting mechanisms.[3,14,16,23-26] On the other hand, the elucidation of the mechanism responsible for the superhydrophobic to superhydrophilic conversion in semiconducting oxide surfaces offers an ideal situation to advance in the understanding of the water condensation behavior and photoactivation of nanostructured surfaces. TiO_2 constitutes the paradigm of photoactive oxide which, widely used for the development of photo-catalysts, biomaterials and self-cleaning surfaces,[23,24,27-32] experiences upon UV irradiation a transformation from hydrophobic to hydrophilic without any apparent modification of surface morphology.

Within such a general context, we aim herein to unravel the factors controlling the wetting and water condensation phenomena on nanostructured surfaces at both the microscopic and molecular levels through an unprecedented “in situ” combined approach by Environmental

Scanning Electron Microscopy (ESEM) and Near Ambient Pressure Photoemission (NAPP) using as one dimensional photoactive model a surface formed by hierarchical TiO_2 domed-nanotubes (NTs) presenting porous tailor-made walls. [33-34]

Results and discussion

TiO_2 domed-nanotubes shown in Figure 1 were fabricated by a full vacuum methodology providing hierarchical 1D microstructure with walls formed by the agglomeration of small nanocolumns. The system presents a singular roughness resulting from their characteristic micro- (nanotubes length: in the range between 2 and 5 um) and nano-scales (nanotube surface: formed by columns with thickness/length below 20/100 nm), as well as a high micro- and meso-porosity.[33-35]

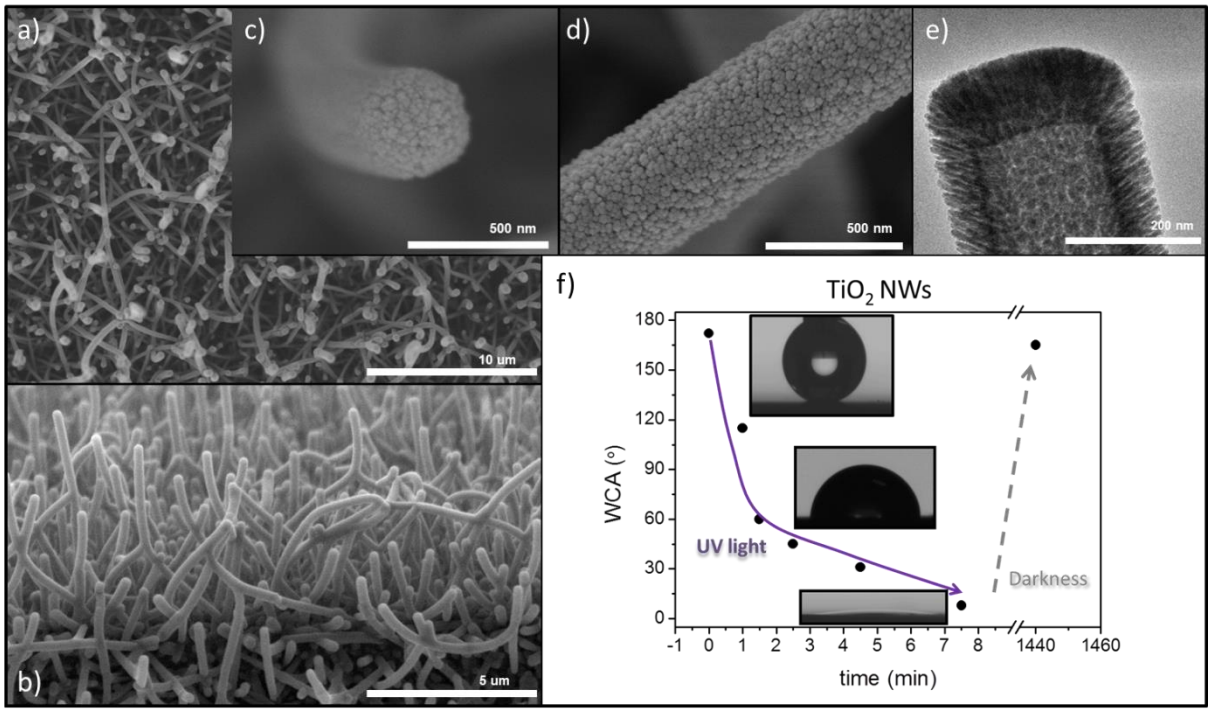

Figure 1. a) and b) Normal view and cross section SEM micrographs of the supported TiO_2 domed-NTs. c) and d) High magnification SEM images of the tip and lateral sides of individual NT. e) TEM micrograph showing the columnar microstructure of the NT walls. f) Evolution of

WCA of the TiO_2 NTs surface just after UV light pre-irradiation under room conditions for the indicated times and latter recovery after storage in dark for one day. Insets present photographs of the water droplets in the initial (top) state and after long UV irradiation (bottom).

In a conventional wetting test, macroscopic sessile droplets placed on the NTs surface under ambient conditions (Fig. 1 a), b)) reveal a superhydrophobic behavior, characterized by water contact angles (WCA) higher than 150º, low contact angle hysteresis (<10º) and a small sliding angle (<2º). In good agreement with previous reports on one-dimensional photoactive surfaces,[13,23,24,35-40] a reversible change from this initial superhydrophobic situation to a superhydrophilic (WCA<10º) state occurs after UV light irradiation of the surface for a time span of several minutes. Figure 1 f) shows the time dependence of WCA for the same TiO_2 NTs surface when subjected to pre-irradiation for increasing periods of time. The obtained decaying curve describes the transition with water droplets bouncing on the surface without any adhesion, to water droplets spreading onto the surface just after a few minutes of pre-irradiation. This transformation of the surface state is reversible just by keeping samples stored in the dark over one day. The initial superhydrophobic state agrees with a metastable Cassie state where the apparent contact angle (θ*) of a surface presenting chemical heterogeneity (in this case TiO_2 and air filling the pores and gaps between NTs) can be calculated by the Caxie-Baxter[9,13,30] equation (Cassie's law) $\cos(\theta^*) = f\cos(\theta) + f - 1$. Where θ corresponds to the WCA of the flat and compact equivalent surface (80º as demonstrated in references 28 and 29) and f to the solid surface forming the liquid-solid interface (ca. of 0.075, obtained by assuming 6 NTs x um^{-2} with a mean diameter of 400 nm and vertical alignment of the NTs). In this way, the calculated value for θ* is 171.5º very closed to the 172º measured by means of the sessile droplet method (Figure 1 f). This behavior is typically found on dual-scaled roughness surfaces. However, for the same surface topography, UV illumination under room conditions leads to a superhydrophilic surface,

typical of a wetted Wenzel state.[13,41] To reach a deeper understanding of this switchable wetting behavior of the TiO_2 NTs and the relationship with the corresponding condensation regimes (dropwise or filmwise), we have carried out a thorough "in situ" characterization study by ESEM for the situations referred as "superhydrophobic" and "superhydrophilic", i.e. comparing as-grown and UV-irradiated nanotubes. Figure 2 gathers micrographs corresponding to normal and cross sectional views of the two wetting states upon progressive condensation of water at low sample temperatures, when the relative humidity of the microscope stage is increased up to induce condensation. For the as-grown NTs (Figure 2 a)-d), i)), when the water vapor pressure is raised close to the relative level of humidity saturation (860Pa at 4ºC), individual water droplets of diameters smaller than 5 μm appear condensed onto the NTs surface (Figure 2 b)). These drops define a minimal pinning of contact line typical of a dropwise condensation behavior.[10-12] Cross section micrographs confirm the formation of isolated droplets on the ~~superhydrophobic~~ TiO_2 NTs surface (Figure 2 c)) due to the hindrance to water spreading depicted by this surface. For small volumes, these microdroplets present a quite spherical shape and grow contacting one or several NTs. In fact, the high resolution image in Figure 2 i) shows the nanotubes immersed within the droplets which indicates that for small droplets the wetting mechanism under condensation follows the Wenzel's law. Droplets sizes increase during the condensation process until they collapse into larger droplets that tend to cover completely the surface. This process must be accounted for by the natural decrease of the ratio between surface and bulk free energies when the nuclei size increases.[42] We have estimated the contact angle for several droplets in Figure 2 c) (see Supporting Information Figure S1) as ~ 69º. Wenzel's equation established that $\cos(\theta^*) = r\cos(\theta)$ where the roughness factor *r* is calculated as the ratio between the total surface area and the geometrical area. In our case, taking into account a density of NWs ca. 6

NWs x um^{-2}, a mean diameter of 400 nm and 2.5 um in length, the roughness factor yields a value $r \sim 2.88$ resulting in $\theta^* \approx 60^o$ in fair agreement with the value obtained from droplets in Figure S1. Therefore, while the wetting regime for sessile droplets under ambient conditions on the macroscopic surface (apparent contact angle) formed by a high density of NTs follows the Cassie-Baxter law, condensation conditions drive to the formation of droplets under the Wenzel state. Thus, during water condensation, the Wenzel state is favored instead of the metastable Cassie state due to nucleation and growth of droplets on top and between the NTs contacting their heads and lateral surfaces. It is also noteworthy in this regard that ambient humidity during apparent contact angle measurements at ambient conditions was rather low (of the order to 20% relative humidity), while water vapor saturation is required to induce condensation. The NAPP experiments reported below provides information about the hydroxylation state of samples under water vapor saturation and therefore under equivalent conditions than those utilized for the environmental SEM experiments in Figure 2. Implications of these water condensation results directly affect the applications of this type of nanostructured material as, for instance, to enhance the mass or heat transfer.[3,5] As a matter of fact, this type of surface will not allow the spontaneous ejection of droplets during condensation with the consequent detriment in the heat transfer process.

After UV light irradiation for 10 minutes, micrographs in Figure 2 e)-h) show a superhydrophilic state characterized by the fast flooding of the NT structure by a continuous liquid film (Figure 2 f)). The cross section analysis (Figure 2 c), g) and j) reveals that now water condensation starts at the bottom of the nanowires in a filmwise way,[10-12] in clear contrast with the water droplet nucleation on the NTs found for the as-grown surface. Eventually, upon

increasing the water pressure in the chamber, the accumulation of water within the superhydrophilic nanostructure continues up to the complete flooding of the NTs (Figure 2 h)).

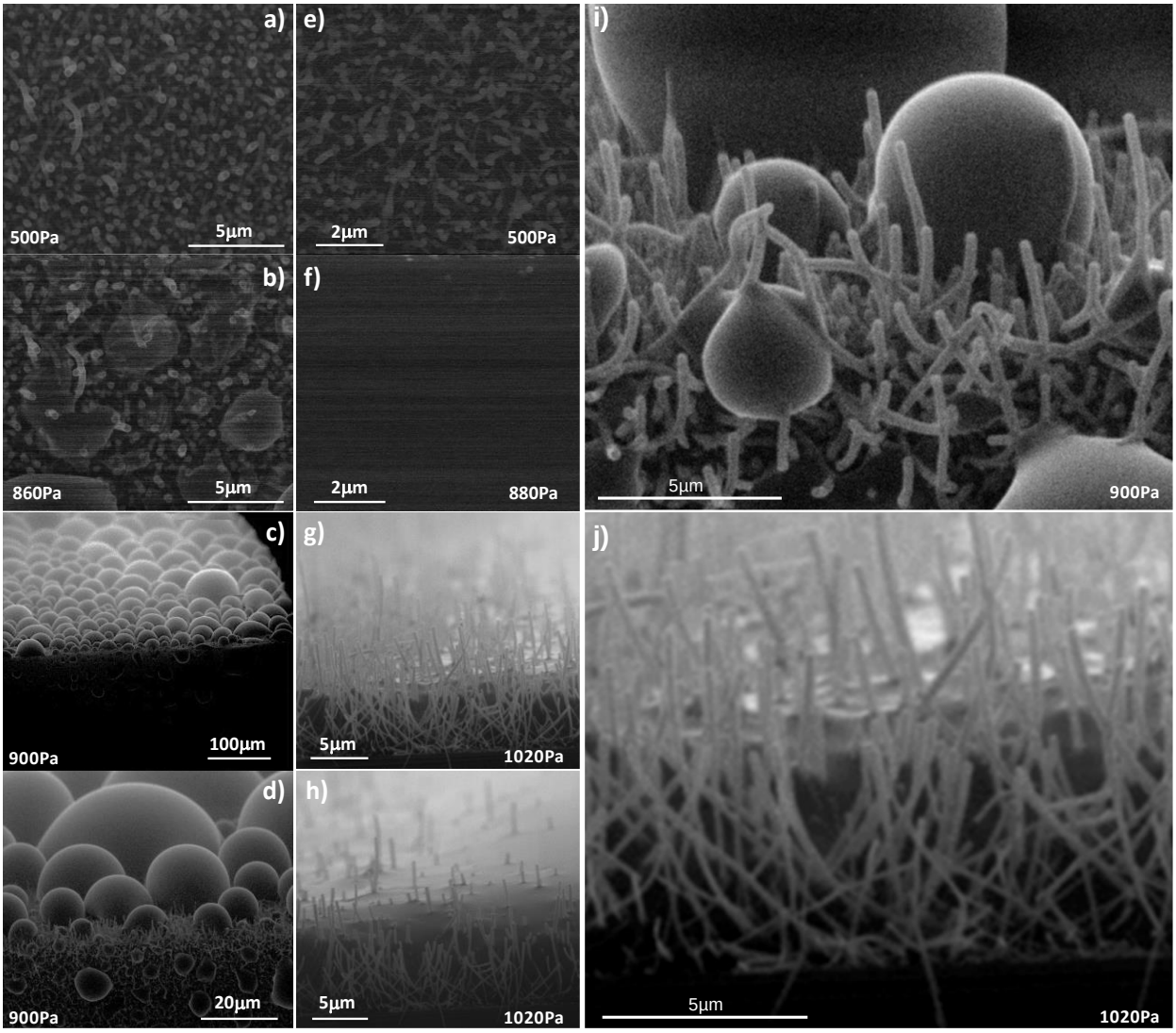

Figure 2. Normal view and cross section ESEM micrographs showing the water condensation on the superhydrophobic TiO_2 NTs surface (a)-d) and i) and after UV illumination (e)-h) and j).

The transition from water droplet to continuous film condensation must be dictated by differences in the TiO_2-water interface energy ($\gamma_{TiO2\text{-}H2O}$) for the apparent superhydrophobic and superhydrophilic states. The question then arises of what specific surface features are induced during UV pre-irradiation and how they affect the interaction with water during condensation.

Another critical issue is the elucidation of the wetting mechanism at the NT-surface, provided that the ESEM resolution under high humidity conditions is not sufficient to assess whether the observed dropwise/filmwise condensation is preceded by a water film or droplet formation at the surface of the NTs or within the porous presenting in the NTs walls (see the columnar nanostructure of the NT wall surfaces in Fig. 1). In addition, in this article we aim to contribute with new experimental insights to solve the controversy generated about the origin of the photo-induced hydrophilicity on metal oxide semiconductors such as TiO_2 and ZnO. Just after the phenomenon was revealed for both anatase and rutile surfaces, Wang et al. [27-29] proposed that UV illumination under ambient conditions induces the formation of oxygen vacancies leading to the dissociation of water to form OH groups responsible for the hydrophilic character. A few years later, it was postulated that the UV modification of the TiO_2 surface followed by water adsorption produced the changes of the OH groups from a twofold binding configuration to onefold direct binding to the Ti sites.[43] However, posterior studies carried out for pristine TiO_2 surfaces under controlled atmosphere (usually in O_2) indicated that UV irradiation has no influence in the uptake of OH groups.[44,45] Within this latter group, are noteworthy the results by Yates et al. on single crystal rutile combining Auger Spectroscopy and Scanning Tunnel Microscopy (STM) studies.[44] These authors concluded that poisoning with carbon residues was the main cause for the increase in surface contact angle on the TiO_2 surface and that the UV driven photo-oxidation of these pollutants was the responsible for the hydrophilic conversion. Herein, trying to get a deeper insight at nano- and molecular-scales we have carried out Near Ambient Pressure Photoemission (NAPP) analyses to in situ follow the surface chemical evolution during the initial states of water condensation. Figure 3 gathers the corresponding C1s peaks recorded under UHV conditions for the as-grown (i.e. characterized by a

superhydrophobic water contact angle of sessile drops and dropwise condensation in Wenzel state) and UV treated samples (i.e. presenting superhydrophilic wetting and filmwise condensation) (see also Table S1 showing C, O and Ti atomic percentages and ratios). The different fitting bands in these C1s spectra can be attributed to -C-C/-C-H (BE ~284.5eV), C-OH/-C-O-C- (BE ~286.0eV), C=O (BE ~287.5eV) and O=C-O/$CO_3^=$ (BE ~288.5eV) species.[46] According to these spectra and surface atomic compositions both surfaces present carbonaceous species, with an approximate ratio C/Ti higher in the irradiated sample (0.27) than in the as-grown nanotubes (0.10). This adventitious carbon should be the result of the synthesis and air manipulation of samples (i.e., exposure to hydrocarbons and other compounds, CO_2, etc.). This result might appear in contradiction with the experiments carried out by Yates et al. showing the removal of carbon species when irradiating the TiO_2 surface in the presence of oxygen,[44] however, it is important to stress a significant difference: we irradiated the NT sample in air, conditions which are known to generate amphiphilic surfaces with low contact angles for both polar and non-polar species.[28] Therefore, we attribute the increment in the C/Ti ratio to the adsorption of carbonaceous compounds during the time of UV irradiation of the TiO_2 surfaces. In this regard, it is worth stressing that the original non-irradiated surface state of the TiO_2 surface exhibits a higher [O=C-O/$CO_3^=$]/[C-C] but a lower [–C-OH]/[C-C] ratio than that after UV irradiation. This evolution can be accounted for by admitting that besides the UV activated adsorption of carbonaceous species from the air, these latter are also progressively photo-oxidized as proposed in the bottom panel of Figure 3.

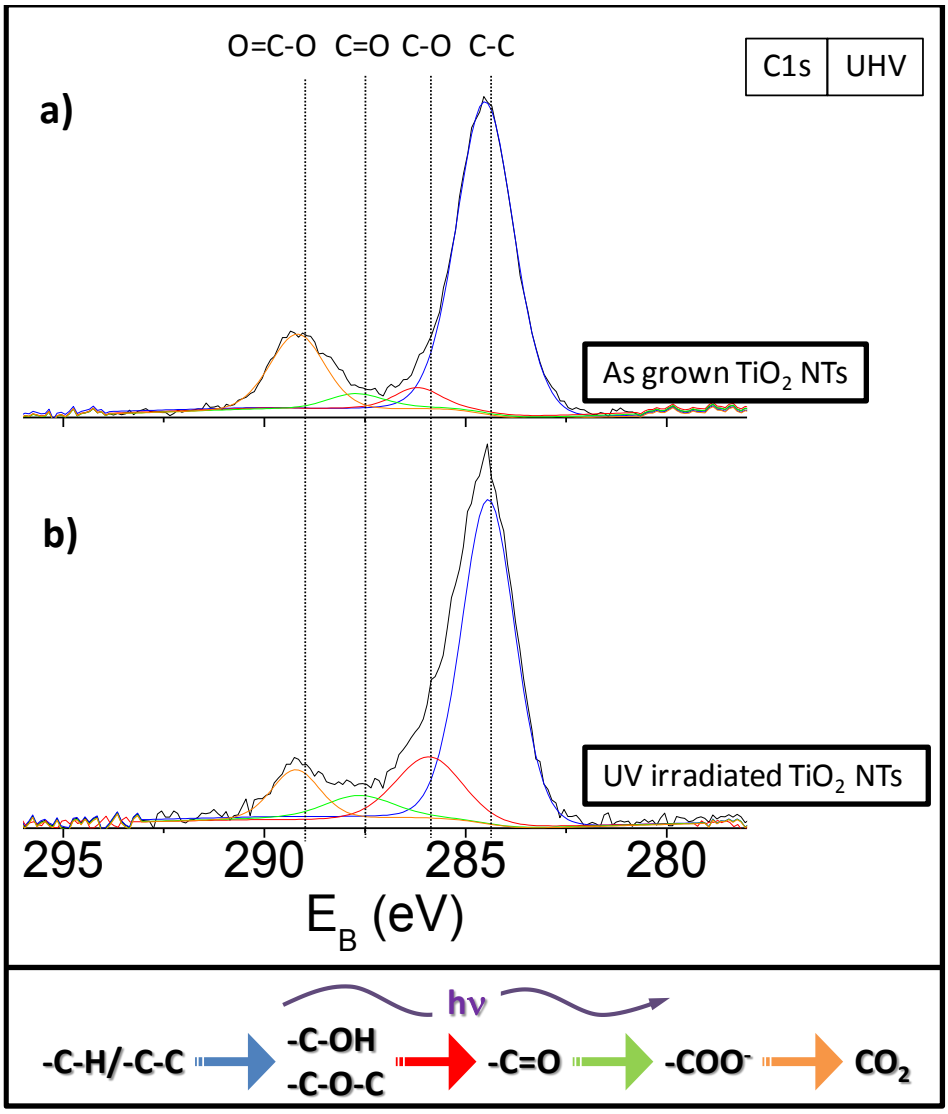

Figure 3. C1s XPS spectra for the superhydrophobic (a) and superhydrophilic (b) TiO_2 NTs surface states. BE positions for the different carbon contributions such as C-C, C-O, C=O and O=C-O/$CO_3^=$ are marked to guide the eyes. Bottom.- Flow chart indicating the evolution of the carbonaceous species under UV irradiation or water condensation (see additional information in Table S1).

Figure 4 collects the O1s spectra of the superhydrophobic and superhydrophilic TiO_2 NTs surfaces recorded "in-situ" under vacuum conditions and after water vapor pressure exposures up

to 350Pa at 6 ºC (see equivalent experiment of a flat thin film surface in Figure S2). It is noteworthy that for both samples the measured Ti/C ratio progressively decreased with the vapor pressure, suggesting the preferential coverage of the Ti sites with OH groups and/or water molecules as explained below. The initial O1s spectra can be described by the contribution of two signals attributed to OH^- groups (binding energy BE~531.2eV, note also the contribution from -CO_x groups depicted in orange color and estimated according to the procedure described in the experimental section) and $O^=$ ions (BE ~529.6eV) bonded to Ti^{4+} cations at the surface[17] (this latter used for intensity normalization). The OH^- signal in the UV pre-illuminated surface has a higher intensity, a feature agreeing with the model by Wang et al. on the surface activation of TiO_2 surfaces UV irradiated in air.[28] As-grown surface also presents OH^- groups likely formed after exposure to ambient conditions prior its insertion in the analysis chamber. For the dropwise condensation regime ~~state~~, dosing 10 Pa into the chamber (Figure 4 b)) leads to a high increase in the intensity of the OH^- component ($OH^-/O^=$ ratio increased from 0.5 to 1.3) and to the development of two new bands at 532.8 eV (H_2O_{ads}) due to adsorbed water and at 535.3 eV (H_2O_g) corresponding to water in the gas phase.[45] These two latter bands grow continuously in intensity when water vapor pressure increases. Unlike the behavior of this ~~superhydrophobic state~~ as-grown surface, in the pre-irradiated sample, the H_2O_{ads} band was smaller after dosing 10 Pa of water vapor and grew much slower with the dose at least during these initials stages of the experiment (Figure 4 f)-h)). It is also worth stressing that the OH^- band only increases moderately up to its saturation ($OH^-/O^=$ ratio increased from 0.8 to 1.2). We tentatively link this different evolution of XPS signals in this NAPP experiment to the formation of very small water droplets on the hydrophobic as-grown NTs surface, and to the condensation of liquid water at the bottom of NTs and within the tube cavities when the sample is in the superhydrophilic state after

UV irradiation. Such a condensation behavior at nanometric scale corresponds to the observations in Figure 2 when either larger water droplets or layers were observed by SEM.

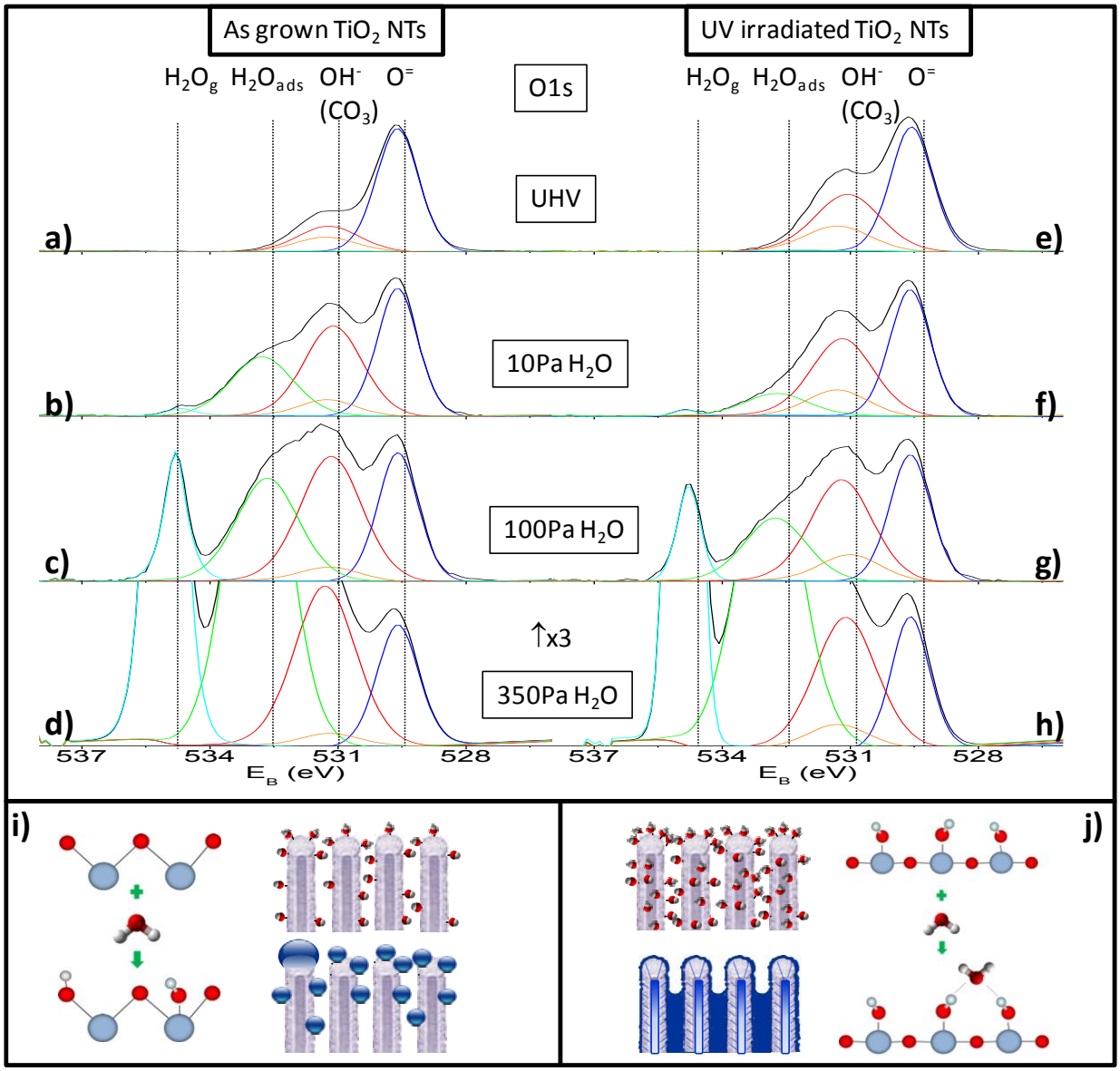

Figure 4. Top.- O1s XPS spectra at vacuum conditions and under water partial pressures as labelled for the as-grown [a)-d)] and UV-irradiated [e)-h)] TiO_2 NTs surfaces. BE positions for the different oxygen contributions such as H_2O_g (water vapor), H_2O_{ads} (adsorbed water), OH^- and $O^=$ are marked to guide the eyes, (with d) and h) vertical scales increased x3). Orange line

corresponds to oxygen in -CO_x species. Bottom.- Pictorial representations of the condensation mechanisms for the dropwise (i) and superhydrophilic filmwise NTs surfaces (j) (blue: Ti atom, red: O atom, white: H atom).

According to the premises of the Tougaard analysis,[47] this hypothesis also agrees with the observation that the background slope in the Ti2p survey XPS spectra (Figure S1, supporting information showing the majority presence of Ti^{4+} species with a minority contribution of Ti^{3+} species in the as-grown sample which are removed after UV irradiation likely by their reaction with water molecules to yield hydrophilic –OH groups) does not change during the progressive covering of the surface with water. A minor attenuation of the Ti2p signal (Figure S1) and a slower progression of the $H_2O_{ads}/O^{=}$ band ratio would also be direct consequences of this different behavior (see the evolution of titanium coverage upon water adsorption as a function of the water partial pressure in Figure S3, indicating that the ratio Ti/H_2O_{ads} remains high for the superhydrophilic surface up to a water pressure in the chamber of around 150 Pa).

It is also interesting to compare the previous results with those obtained by performing the NAPP experiment on a TiO_2 thin film surface (Figure S4), i.e. fabricated under the same experimental conditions on a flat substrate. Water contact angle for this surface estimated by sessile droplet method is about 90º, reaching superhydrophilicity after UV irradiation during several minutes. Although this surface does not present a superhydrophobic wetting behavior, the qualitative evolutions of the O1s peaks for as-grown and irradiated thin films are similar to those found for the NTs sample.

Taking together all these experimental evidences, Figure 4 bottom) shows a schematic representation of the wetting mechanism for the as-grown and irradiated NTs surfaces at the initial

stages of water condensation. According to this scheme, upon water vapor exposure at 10 Pa, hydroxyl groups extensively accumulate on the surface of the as-grown sample, where they promote water molecules adsorption and condensation in the form of small droplets at the NTs tips and lateral surfaces. Following the ideas deduced from the analysis of Figure 2, these droplets are likely in a Wenzel state, where condensed water would also partially cover the gaps between the nanocolumns in the NTs shells (no shown in the schematic on the sake of simplicity). The progressive size increase of these droplets would be the responsible for the observed attenuation of the Ti2p signal and the increase in the H_2O_{ads} band. Onto the superhydrophilic surface, the concentration of hydroxyl groups is already quite significant before water exposure, and condensation of water droplets does not occur at the tip surface zones of the NTs (i.e., condensed water is then undetected by XPS) but in the interior of the tubes and in the intercolumnar space in the NTs-shells as well as in the gaps between NTs. In previous articles, we demonstrated that the equivalent columnar thin film layer (see Figure S5) presents a pore size distribution ranging from micro (pore diameter below 2 nm, within the columns) to mesoporous (diameter between 2 and 50 nm, within and between the columns).[35] Columns mean diameter in the NTs walls is smaller than that measured in the equivalent thin film, therefore, we can assume that the pore size distribution corresponding to the NTs walls microstructure is also in the range of the micro and mesopores. Thus, the presence of condensed water in the micro and mesopores in the NTs shells and interior of the NTs at this relative low water pressure is in good agreement with the premises of the inverse Kelvin effect[48-50] which predicts a lower saturation water vapor pressure required for water condensation on porous hydrophilic structures with respect to plane and compact surfaces. In consequence, high water coverage of the NTs is reached for the highest pressure situation, i.e. 350Pa at low temperature, for hydrophobic and superhydrophilic states (Figure 4 d) and h)). These

conditions correspond to the maximum intensity of the H_2O_{ads} band compared to the $O^{=}$ and OH^{-} contributions, in addition to the highest H_2O_g signal coming from the environment. Evolution of the composition and different oxygen bands on both surfaces with the water vapor pressure is fully reversible. Since the thin film surface does not reach superhydrophobic water contact angles for the as-grown conditions and the total surface area is much smaller than that in the NTs samples, the surface becomes completely covered by water at 350 Pa. In fact, the photoemission band corresponding to $O^{=}$ is barely visible at this given pressure for both as-grown and UV-irradiated surfaces.

However, in the previous considerations relating NAPP spectra and FESEM condensation behavior it is unclear why the OH- groups formed on the as grown samples during their exposure to water vapor and those already existing in UV-irradiated samples should induce a different water condensation behavior. We assume that the different acidity of the OH groups in the two cases is the main reason for the observed differences. In fact, it was proposed that hydroxylation of TiO_2 single crystals may occur through the formation of basic and/or acid Ti-OH species, respectively characterized by the direct bonding of OH^{-} groups to 5-coordinated titanium ions or the protonation of bridging oxygen at Ti-O-Ti sites. The O1s XPS bands of these hydroxyl groups are shifted by +2.5 eV and +1.3 eV with respect to the position of the oxide ($O^{=}$) main peak.[51] For the as grown TiO_2 NTs, the OH^{-} bands after water vapor exposure (Figure 4 b) and f)) detected in our experiment are broader than those corresponding to the vacuum conditions and shifted by +1.6 eV with respect to the $O^{=}$ band. This fact, joined to the slightly higher width of the OH band in the superhydrophilic state (1.78eV against 1.66eV for the as-grown surface), points to a heterogeneous surface hydroxylation which, in the irradiated sample, will count with a higher contribution of acid groups (see schematics in Figure 4 Bottom). These acidic groups

would favor the diffusion of water molecules that, in this way, would condense at the bottom of the NTs. The more basic OH groups in the as-grown NTs would not promote water diffusion to the interior of NTs and therefore would condense in the form of droplets at the tips surface.

Conclusions

Taking into account the results and recent precedents in the literature, we propose the processes gather in Figure 4 i) and j) as responsible for the wetting of as-grown and pre-irradiated nanotubes correspondently. The main mechanistic assumption in the scheme in Figure 4 i) and j) is that water adsorption is different on the hydrophobic and hydrophilic surface state not only because this last contains a higher concentration of hydroxyl groups, but also due to a different surface arrangement of $O^{=}$ and Ti^{4+} species at the surface.[52] It is known that water dissociative adsorption onto the oxygen terminated TiO_2 (001) surface plane requires an energy of 184.7 kJ/mol, which is higher than that needed for hydroxylation of other surface planes containing both Ti and O ions (e.g. lower than 70kJ/mol for TiO_2 (100) and (101)). Nevertheless, the previous hydration of the surface decreases the adsorption energy by more than 45%. In this way, we think that in our NT system a hydroxylated surface due to UV preirradation is less reactive upon low vapor pressure water exposure and therefore less prone to highly increase its surface hydroxylation as it happens with the hydrophobic state (note however that almost equivalent hydroxylation levels are found at higher vapor pressures, cf. Figure 4 d) and f)). On this superhydrophilic surface, water molecules tend to strongly interact through the formation of hydrogen bonds, this leading to its diffusion to the interior of the NTs cavities and voids where, favored by capillary and inverse Kelvin effects, it starts to condense even at the lowest vapor pressures of our experiment (Figure 4j)). In this regard, it is worth mentioning that previous experiments with metals[53] and single rutile crystal surfaces[54] have confirmed the formation of

one-dimensional H-bonded water chains governing by diffusion and adsorption of OH groups and water molecules onto pentacoordinated Ti surface sites, a situation which is compatible with a superhydrophilic state. Therefore, without discarding a contribution according to the suggestion of Yates et al. in the sense that carbonaceous species may contribute to increase the wetting contact angle of water on pristine, non-irradiated, TiO_2,[44] our "in situ" experiments with photoactive oxide NTs support the model of Watanabe et al. and other authors [28,44,55] in the sense that the dissociation of water molecules from air is the main factor contributing to enhance hydrophilicity. This conclusion is also extensible to the similar behavior of other photoactive 1D nanostructured surfaces, like supported ZnO nanowires.[36-37] Our findings also support a revised description of the dropwise water condensation onto apparent superhydrophobic nanostructures (i.e., presenting WCA > 150º, low hysteresis and sliding angles for sessile drops under ambient conditions) which would be compatible with the metastable Cassie-Baxter state for sessile droplets and Wenzel state for microdroplets formed after water condensation. In addition, we have demonstrated the adsorption of hydroxyl groups on the topmost surface layer of the NTs walls. Without implying any morphological transformation, this wetting state can be drastically transformed into superhydrophilic if the nature and amount of adsorbed OH^- groups is changed during irradiation. This would favor a diffusive water adsorption and migration towards the bottom of voids where capillary forces contribute to its condensation. Results gathered in this work might also add critical information to other interesting issues, like fabrication of water harvesting systems, time evolution of photoinduced hydrophilic surfaces and their dependence on the illumination conditions,[56] as well as to the industrial fabrication of anti-freezing surfaces.[19]

EXPERIMENTAL METHODS

Sample preparation: Vertically oriented domed-TiO_2 nanotubes samples, with typical individual thicknesses in the range of 200-500 nm and a length of several microns, were fabricated on Si(100) substrates by a full vacuum and plasma deposition method carried out at mild temperatures.[33,34] The samples were handled in air after their preparation and stored in a desiccator until their use, entailing UV irradiation in air and insertion in the ESEM or NAPP chambers. See additional details in the Supporting Information.

Characterization: Static water contact angle (WCA) measurements were provided by a Data Physics setup by depositing bidistilled water drops of 1μL. Samples were preilluminated for different periods of time with a UV lamp (Xe) with a spectrum power of $2Wcm^{-2}$. Environmental scanning electron microscope (ESEM) experiments were performed in Quanta FEG250 from FEI by placed the sample on a Peltier stage and controlling the water vapor pressure in the system. Temperature was stabilized to 4 or 8 °C for condensation in the superhydrophobic or superhydrophilic states respectively. Near Ambient Pressure Photoemission (NAPP) spectrometer is located at the BL-24 CIRCE undulator beamline, in ALBA synchrotron light source (Sant Cugat del Vallés, Spain); it is equipped with a Phoibos NAP150 XPS analyzer (SPECS) and a differential pumping system for operating at a pressure range from UHV up to 5 mbar of water vapor. The beam spot size at the sample is around 100 x 20 μm^2. Water condensation conditions were reached by cooling the sample with a Peltier element at a temperature of 6ºC. Samples were excited with photons of 880 eV and the emitted photoelectrons were analyzed with a pass energy of 10 eV. XPS measurements were performed taking a new pristine surface region close to the previously measured one (~100μm) for each different ambient condition to avoid a possible beam damage. Fitting analysis of the O1s and C1s spectra was carried out by using Gaussian–Lorentzian bands after subtraction of Shirley-

type backgrounds. For this fitting analysis the contribution of oxygen atoms bonded to carbon (i.e., CO_x species) was determined from the intensity of oxidized carbon groups in the C1s spectrum. The difference in the cross section of C1s and O1s signals, as well as the atomic ratios between oxygen and carbon in the different species has been taken into account to estimate the intensity of this oxygen band. Since the position of this small intensity band was left free during fitting small shifts in BE position were observed, although these changes did not affect the main feature of the experiment related to the increase in the intensity of OH^- bands upon water adsorption.

Supporting Information. Additional experimental details and XPS characterization.

The following files are available free of charge.

SupportingInformation.pdf

AUTHOR INFORMATION

Corresponding Author

*anaisabel.borras@icmse.csic.es *mclopez@icmse.csic.es

Author Contributions

The manuscript was written through contributions of all authors. All authors have given approval to the final version of the manuscript.

ACKNOWLEDGMENTS

We thank the Junta de Andalucia (TEP8067, FQM-196, and P12-FQM-2265), the European Regional Development Funds program (EU-FEDER), the AEI and MINECO (projects MAT2013-

40852-R, MAT2013-42900-P, MINECO-CSIC 201560E055 and MAT2016-79866-R) for financial support.

REFERENCES

[1] He, M.; Wang, J.; Li, H.; Song, Y. Super-Hydrophobic Surfaces to Condensed Micro-Droplets at Temperatures Below the Freezing Point Retard Ice/Frost Formation. *Soft Matter* **2011**, *7*, 3993

[2] Nakata, K.; Ochiai, T.; Murakami, T.; Fujishima, A. Photoenergy Conversion with TiO_2 Photocatalysis: New Materials and Recent Applications. *Electrochimica Acta* **2012**, *84*, 103.

[3] Enright, R.; Miljkovic, N.; Alvarado, J. L.; Kim, K.; Rose, J. W. Dropwise Condensation on Micro- and Nanostructured Surfaces. *Nanoscale Microscale Thermphys. Eng.* **2014**, **18**, 223.

[4] Miljkovic, N.; Preston, D. J.; Enright, R.; Wang, E. N. Electric-Field-Enhanced Condensation on Superhydrophobic Nanostructured Surfaces. *ACS Nano* **2013**, *12*, 11043.

[5] Chen, C. H.; Cai, Q.; Tsai, C.; Chen, C. L. Dropwise condensation on superhydrophobic surfaces with two-tier roughness. *Appl. Phys. Lett.* **2007**, *90*, 173108.

[6] Bekou, S.; Mattia, D. Wetting of Nanotubes. *Current Opinion in Coll. Inter. Sci.* **2011**, *16*, 259.

[7] Narhe, R. D.; Beysens, D. A. Nucleation and Growth on a Superhydrophobic Grooved Surface. *Phys. Rev. Letters* **2004**, *93*, 076103.

[8] Enright, E.; Milijkovic, N.; Al-Obeidi, A.; Thompsom, C. V.; Wang, E. N. Condensation on Superhydrophobic Surfaces: The Role of Local Energy Barriers and Structure Length Scale. *Langmuir* **2012**, *28*, 14424.

[9] Cassie, A. B. D.; Baxter, S. Wettability of Porous Surfaces. *Transactions Faraday Soc.* **1944**, *40*, 546.

[10] Dendooven, J.; Devloo-Casier, K.; Ide, M.; Grandfield, K.; Kurttepeli, M.; Ludwig, K. F.; Bals, S.; Van Der Voort, P.; Detavernier, C. Atomic Layer Deposition-Based Tuning of the Pore Size in Mesoporous Thin Films Studied by in Situ Grazing Incidence Small Angle X-Ray Scattering. *Nanoscale* **2014**, *6*, 14991.

[11] Hou, Y.; Yu, M.; Chen, X.; Wang, Z.; Yao, S. Recurrent Filmwise and Dropwise Condensation on a Beetle Mimetic Surface. *ACS Nano* **2015**, *9*, 71.

[12] Tian, J.; Zhu, J.; Guo, H. Y.; Li, J.; Feng, X. Q.; Gao, X. Efficient Self-Propelling of Small-Scale Condensed Microdrops by Closely Packed ZnO Nanoneedles. *J. Phys. Chem. Letters* **2014**, *5*, 2084.

[13] Macias-Montero, M.; Borras, A.; Alvarez, R.; Gonzalez-Elipe, A. R. Following the Wetting of One-Dimensional Photoactive Surfaces. *Langmuir* **2012**, *28*, 15047.

[14] Chu, K. H.; Xiao. R.; Wang, E. N. Uni-directional liquid spreading on asymmetric nanostructured surfaces. *Nature Mater.* **2010**, *9*, 413.

[15] Drelich, J.; Wilbur, J. L.; Miller, J. D. Whitesides, G. M. Contact Angles for Liquid Drops at a Model Heterogeneous Surface Consisting of Alternating and Parallel Hydrophobic/Hydrophilic Strips. *Langmuir* **1996**, *12*, 1913.

[16] Xia, D.; Johnson, L. M.; Lopez, G. P. Anisotropic Wetting Surfaces with One-Dimesional and Directional Structures: Fabrication Approaches, Wetting Properties and Potential Applications. *Adv. Mater.* **2012**, *24*, 1287.

[17] Zhang, Y. L.; Xia, H.; Kim, E.; Sun, H. B. Recent developments in superhydrophobic surfaces with unique structural and functional properties. *Soft Matter* **2012**, *8*, 11217.
[18] Babu, D. J.; Varanakkottu, S. N.; Eifert, A.; Koning, D.; Cherkashinin, G.; Hardt, S.; Schneider, J. J. Inscribing Wettability Gradients Onto Superhydrophobic Carbon Nanotube Surfaces. *Adv. Mater. Interfaces* **2014**, *1*, 1300049.
[19] Kreder, M. J.; Alvarenga, J.; Kim, P.; Aizenberg, J. Design of anti-icing surfaces: smooth, textured or slippery? *Nature Rev.* **2016**, *1*, 1;
[20] Sojoudi, H.; Wang, M.; Boscher, N. D.; McKinley, G. H.; Gleason, K. K. Durable and Scalable Icephobic Surfaces: Similarities and Distinctions from Superhydrophobic Surfaces. *Soft Matter* **2016**, *12*, 1938
[21] Maitra, T.; Jung, S.; Giger, M. E.; Kandrical, V.; Ruesch, T.; Poulikakos, D. Superhydrophobicity vs. Ice Adhesion: The Quandary of Robust Icephobic Surface Design. *Adv. Mater. Interfaces* **2015**, *2*, 1500330.
[22] Golovin, K.; Kobaku, S. P. R.; Lee, D. H.; DiLoreto, E. T.; Mabry, J. M.; Tuteja, A. Designing durable icephobic surfaces. *Sci. Adv.* **2016**, *2*, e1501496.
[23] Hu, Z.; Zhang, X.; Liu, Z.; Huo, K.; Chu, P. K.; Zhai, J.; Jiang, L. Regulating Water Adhesion on Superhydrophobic TiO2 Nanotube Arrays. *Adv. Funct. Mater.* **2014**, *24*, 6381.
[24] Lai, Y.; Pan, F.; Xu, C.; Fuchs, H.; Chi, L. In Situ Surface- Modification- Induced Superhydrophobic Patterns with Reversible Wettability and Adhesion. *Adv. Mater.* **2013**, *25*,1682.
[25] Ma, X.; Cao, M.; Teng, C.; Li, H.; Xiao, J.; Liu, K.; Jiang, L. In Situ Surface-Modification-Induced Superhydrophobic Patterns with Reversible Wettability and Adhesion. *J. Mater. Chem. A* **2015**, *3*, 15540.
[26] Hong, X.; Gao, X.; Jiang, L. Application of Superhydrophobic Surface with High Adhesive Force in No Lost Transport of Superparamagnetic Microdroplet. *J. Amer. Chem. Soc.* **2007**, *129*, 1478.
[27] Wang, R.; Hashimoto, K.; Fujishima, A.; Chikuni, M.; Kojima, E.; Kitamura, A.; Shimohigoshi, M.; Watanabe, T. Photogeneration of Highly Amphiphilic TiO_2 Surfaces. *Adv. Mater.* **1998**, *10*, 135
[28] Wang, R.; Hashimoto, K; Fujishima, A. Light-induced amphiphilic surfaces. *Nature* **1997**, *388*, 431- 432.
[29] Takeda, S.; Fukawa, M. Role of surface OH groups in surface chemical properties of metal oxide films. *Mater. Sci. Eng. B* **2005,** *119*, 265-267.
[30] Miwa, M.; Nakajima, A.; Fujishima, A.; Hashimoto, K.; Watanabe, T. Effects of the Surface Roughness on Sliding Angles of Water Droplets on Superhydrophobic Surfaces. *Langmuir* **2000**, *16*, 5754-5760.
[31] Parkin, I. P.; Palgrave, R. G. Self-Cleaning Coatings. *J. Mater. Chem.* **2005**, *15*, 1689.
[32] Nakata, K.; Fujishima, A. TiO_2 photocatalysis: Design and applications. *J. Photochem. Photobiolog. C* **2012**, *13*, 169.
[33] Macias-Montero, M.; Filippin, A. N.; Saghi, Z.; Aparicio, F. J.; Barranco, A.; Espinos, J. P.; Frutos, F.; Gonzalez-Elipe, A. R.; Borras, A. Vertically Aligned Hybrid Core/Shell Semiconductor Nanowires for Photonics Applications. *Adv. Func. Mater.* **2013**, *23*, 5981.
[34] Filippin, A. N.; Macias-Montero, M.; Saghi, Z.; Idigoras, J.; Burdet, P.; Barranco, A.; Midgley, P.; Anta, J. A.; Borras, A. Vacuum Template Synthesis of Multifunctional Nanotubes with Tailored Nanostructured Walls. *Sci. Rep.* **2016**, *6*, 20637
[35] Borras, A.; Alvarez, R.; Sanchez-Valencia, J. R.; Ferrer, J.; Gonzalez-Elipe, A. R. Critical thickness and nanoporosity of TiO_2 optical thin films. *Micro. Meso. Mater.* **2012**, *160*, 1.

[36] Feng, X.; Feng, L.; Jin, M.; Zhai, J.; Jiang, L.; Zhu, D. Reversible super-hydrophobicity to super-hydrophilicity transition of aligned ZnO nanorod films. *J. Amer. Chem. Soc.* **2004**, *126*, 62.
[37] Macias-Montero, M.; Borras, A.; Saghi, Z.; Romero-Gomez, P.; Sanchez-Valencia, J. R.; Gonzalez, J. C.; Barranco, A.; Midgley, P.; Cotrino, J.; Gonzalez-Elipe, A. R. Superhydrophobic Supported Ag-NPs@ZnO-Nanorods with Photoactivity in the Visible Range. *J. Mater. Chem.* **2012**, *22*, 1341.
[38] Macias-Montero, M.; Borras, A.; Romero-Gomez, P.; Cotrino, J.; Frutos, F.; Gonzalez-Elipe, A. R. Plasma Deposition of Superhydrophobic Ag@TiO_2 Core@Shell Nanorods on Processable Substrates. *Plasma Proc. Polymers* **2014**, *44*, 164.
[39] Rico, V.; Lopez, C.; Borras, A.; Espinos, J. P.; Gonzalez-Elipe, A. R. Effect of visible light on the water contact angles on illuminated oxide semiconductors other than TiO_2. *Solar Ener. Mater. Solar Cells* **2006**, *90*, 2944.
[40] Borras, A.; Barranco, A.; Gonzalez-Elipe, A. R. Reversible superhydrophobic to superhydrophilic conversion of Ag@TiO_2 composite nanofiber surfaces. *Langmuir* **2008**, *24*, 8021.
[41] Wenzel, R. N. Resistance of Solid Surfaces to Wetting by Water. *Ind. Eng. Chem.* **1936**, *28*, 988.
[42] Miljkovic, N.; Enright, R.; Wang, E. N. Effect of Droplet Morphology on Growth Dynamics and Heat Transfer During Condensation on Superhydrophobic Nanostructured Surfaces. *ACS Nano* **2012**, *6*, 1776.
[43] Sakai, N.; Fujishima, A.; Watanabe, T. Hashimoto, K. Quantitative evaluation of the photoinduced hydrophilic conversion properties of TiO_2 thin film surfaces by the reciprocal of contact angle. *J. Phys. Chem. B* **2003**, *107*, 1028.
[44] Yates Jr, J. T. Photochemistry on TiO_2: Mechanisms Behind the Surface Chemistry. *Surf. Sci.* **2009**, *603*, 1605.
[45] Lampimäki, M.; Schreiber, S.; Zelenay, V.; Křepelová, A.; Birrer, M.; Axnanda, S.; Mao, B.; Liu, Z.; Bluhm, H.; Ammann, M.; Exploring the Environmental Photochemistry on the TiO_2(110) Surface in Situ by near Ambient Pressure X-Ray Photoelectron Spectroscopy. *J. Phys. Chem. C* **2015**, *119*, 7076.
[46] Zhao, D.; Sheng, G.; Chen, C.; Wang, X. Enhanced photocatalytic degradation of methylene blue under visible irradiation on graphene@TiO_2 dyade structure. *Appl. Catal. B* **2012**, *111-112*, 303.
[47] Tougaard, S. Surface nanostructure determination by x- ray photoemission spectroscopy peak shape analysis. *J. Vacuum Sci. Technol. A* **1996**, *14*, 1415.
[48] Sjorgren, S.; Gysel, M.; Weingartner, E.; Baltensperger, U.; Cubison, M. J.; Coe, H.; Zardini, A. A.; Marcolli, C.; Krieger, U. K.; Peter, T. Hygroscopic growth and water uptake kinetics of two-phase aerosol particles consisting of ammonium sulfate, adipic and humic acid mixtures. *Aerosol Sci.* **2007**, *38*, 157.
[49] Wagner, R.; Kiselev, A.; Möhler, O.; Saathoff, H.; Steinke, I. Pre-activation of ice-nucleating particles by the pore condensation and freezing mechanism. *Atmos. Chem. Phys.* **2016**, *16*, 2025.
[50] Marcolli, C. Deposition nucleation viewed as homogeneous or immersion freezing in pores and cavities. *Atmos. Chem. Phys. Discuss.* **2013**, *13*, 16367.
[51] Perron, H.; Vandenborre, J.; Domain, C.; Drot, R.; Roques, J.; Simoni, E.; Ehrhardt, J. J.; Catalette, H.; Combined Investigation of Water Sorption on TiO_2 Rutile (1 1 0) Single Crystal Face: XPS vs. Periodic DFT. *Surf. Sci.* **2007**, *601*, 518.
[52] Almeida, A. R.; Calatayud, M.; Tielens, F.; Moulijn, J. A.; Mul, G. Combined ATR-FTIR

and DFT Study of Cyclohexanone Adsorption on Hydrated TiO_2 Anatase Surfaces. *J. Phys. Chem. C* **2011**, *115*, 14164.
[53] Yamamoto, S.; Andersson, K.; Bluhm, H.; Ketteler, G.; Starr, D. E.; Schiros, T.; Ogasawara, H.; Pettersson, L. G. M.; Salmeron, M.; Nilsson, A. Hydroxyl-Induced Wetting of Metals by Water at near-Ambient Conditions. *J. Phys. Chem. C* **2007**, *111*, 7848.
[54] Lee, J.; Sorescu, D. C.; Deng, X.; Jordan, K. D. Water Chain Formation on TiO_2(110). *J. Phys. Chem. Letters* **2013**, *4*, 53.
[55] Li, W.; Guo, T.; Meng, T.; Huang, Y.; Li, X.; Yan, W.; Wang, S.; Li, X. Enhanced Reversible Wettability Conversion of Micro-Nano Hierarchical TiO_2/SiO_2 Composite Films under UV Irradiation. *Appl. Surf. Sci.* **2013**, *283*, 12.
[56] Rudakova, A. V.; Oparicheva, U. G.; Grishina, A. E.; Maevskaya, M. V.; Emeline, A. V.; Bahnemann, D. W. Dependences of ZnO Photoinduced Hydrophilic Conversion on Light Intensity and Wavelengths. *J. Phys. Chem. C* **2015**, *119*, 9824.

TOC GRAPHIC